



1 **Unleashing the Potential of Geostationary Satellite Observations in Air**

2 **Quality Forecasting Through Artificial Intelligence Techniques**

3 Chengxin Zhang¹, Xinhan Niu¹, Hongyu Wu², Zhipeng Ding², Ka Lok Chan³, Jhoon Kim⁴,

4 Thomas Wagner⁵, Cheng Liu^{1,6,7*}

5 ¹Department of Precision Machinery and Precision Instrumentation, University of Science and
6 Technology of China, Hefei, 230026, China

7 ²School of Environmental Science and Optoelectronic Technology, University of Science and
8 Technology of China, Hefei, 230026, China

9 ³Rutherford Appleton Laboratory Space, Harwell Oxford, United Kingdom

10 ⁴Department of Atmospheric Sciences, Yonsei University, Seoul, Republic of Korea

11 ⁵Satellite Remote Sensing Group, Max Planck Institute for Chemistry, Mainz, Germany

12 ⁶Key Laboratory of Environmental Optics and Technology, Anhui Institute of Optics and Fine
13 Mechanics, Chinese Academy of Sciences, Hefei, 230031, China

14 ⁷Key Laboratory of Precision Scientific Instrumentation of Anhui Higher Education Institutes,
15 University of Science and Technology of China, Hefei, 230026, China

16

17 *Correspondence: Cheng Liu (chliu81@ustc.edu.cn)

18

19



20 **Abstract.**

21 Air quality forecasting plays a critical role in mitigating air pollution. However, current
22 physics-based air pollution predictions encounter challenges in accuracy and spatiotemporal
23 resolution due to limitations in the understanding of atmospheric physical mechanisms,
24 observational constraints, and computational capacity. The world's first geostationary satellite
25 UV-Vis spectrometer, i.e., the Geostationary Environment Monitoring Spectrometer (GEMS),
26 offers hourly measurements of atmospheric trace gas pollutants at high spatial resolution over
27 East Asia. In this study, we successfully incorporate Geostationary satellite observations into
28 a neural network model (GeoNet) to forecast full-coverage surface nitrogen dioxide (NO₂)
29 concentrations over eastern China at 4-hour intervals for the next 24 hours. GeoNet leverages
30 spatiotemporal series of satellite NO₂ observations to capture the intricate relationships among
31 air quality, meteorology, and emissions in both temporal and spatial domains. Evaluation
32 against ground-based measurements demonstrates that GeoNet accurately predicts diurnal
33 variations and spatial distribution details of next-day NO₂ pollution, yielding the coefficient of
34 determination of 0.68 and root mean square of error of 12.31 µg/m³, significantly surpassing
35 traditional air quality model forecasts. The model's interpretability reveals that geostationary
36 satellite observations notably improve NO₂ forecast capability more than other input features,
37 especially over polluted regions. Our findings demonstrate the significant potential of
38 geostationary satellite observations in artificial intelligence-based air quality forecasting, with
39 implications for early warning of air pollution events and human health exposure.

40 **Keywords:** air quality forecast; deep learning; health impact; satellite remote sensing;
41 nitrogen dioxide;



42 **1 Introduction**

43 Since the industrial revolution, numerous countries worldwide have encountered severe
44 air pollution issues such as photochemical ozone smog and haze pollution (Hong et al., 2019),
45 which significantly affect human health, crop yields, and the global environment (Guarin et al.,
46 2024; Manisalidis et al., 2020; Sathe et al., 2021). Recent studies have shown that both long-
47 term and short-term exposure to air pollutants such as nitrogen dioxide (NO₂) can significantly
48 affect human health, especially the respiratory system (Meng et al., 2021). Accurate and high
49 spatial resolution predictions of air pollutant concentrations can provide critical information
50 for sensitive persons to mitigate health risks. In recent decades, the advancement of
51 atmospheric monitoring and modeling has enabled significant progress in air quality
52 forecasting based on our understanding of atmospheric physics and chemistry (Peuch et al.,
53 2022). Air pollution forecasting not only facilitates responses to environmental health risks but
54 also improves the accuracy of climate and weather simulations (Makar et al., 2015). However,
55 due to our still limited understanding of atmospheric mechanisms and limited observational
56 and emission constraints, existing air quality forecasts based on physical or statistical models
57 still face challenges in terms of temporal, spatial, and accuracy aspects (Campbell et al., 2022;
58 Zhong et al., 2021).

59 Artificial Intelligence (AI) technology has made breakthroughs in the field of Earth
60 science (Boukabara et al., 2020; Zhong et al., 2021), particularly excelling in addressing
61 complex problems that are challenging for traditional physical paradigms to simulate (Irrgang
62 et al., 2021), such as weather and climate forecasting (Andersson et al., 2021). Concerning
63 meteorological data, some large-scale deep learning models have surpassed the predictive
64 capabilities of existing numerical weather models to some extent, examples include Climax
65 (Nguyen et al., 2023), Pangu-Weather (Bi et al., 2023), and GraphCast (Lam et al., 2023).
66 Despite significant progress and impressive performance achieved in meteorological variables



67 forecasting with AI methods, there are still limitations in predicting atmospheric pollutant
68 compositions. Compared to meteorological parameters, the prediction of air pollutant
69 concentrations is affected by synoptic meteorology, chemistry, and anthropogenic emission
70 activities, usually with more complex driven mechanisms and associated uncertainties. Current
71 AI-based air quality forecasts often involve time series predictions at a limited number of
72 observation stations, rather than full-coverage predictions over the entire spatial domain (Du
73 et al., 2021). This is primarily due to the lack of effective air quality observations with high
74 temporal and spatial resolution simultaneously.

75 While past polar-orbiting satellite observations have provided extensive coverage of
76 atmospheric pollutant distributions such as nitrogen dioxide (NO₂), sulfate dioxide (SO₂),
77 ozone (O₃), and aerosols, they are limited to once-daily overpasses and usually affected by
78 clouds (Chan et al., 2023; Van Geffen et al., 2022). This frequency usually exceeds the
79 chemical lifetimes of many reactive gas pollutants like NO₂, making it challenging to offer
80 effective observational constraints for machine learning short-term air quality forecasting
81 (Shah et al., 2020). In February 2020, the world's first geostationary satellite payload for air
82 pollution monitoring, the Geostationary Environment Monitoring Spectrometer (GEMS),
83 began to provide high-coverage and high-precision air quality observations at an hourly rate
84 for the East Asian region (J. Kim et al., 2020). The dynamic processes of air pollutants
85 including emission, transformation, and transport can be observed by the geostationary satellite
86 during the daytime. This monitoring capability may advance data-driven air quality forecasting
87 such as machine learning techniques by offering unprecedented observational constraints with
88 high spatial and temporal coverage. Recent observing system simulation experiments (OSSE)
89 indicate that assimilating trace gas observations by geostationary satellites into chemical
90 models can effectively improve surface ozone simulations (Shu et al., 2023), nitrogen oxides
91 (NO_x), and emission estimates (Hsu et al., 2024).



92 Here, based on the unprecedented temporal resolution of the GEMS satellite (J. Kim et
93 al., 2020), we incorporated Geostationary satellite remote sensing of tropospheric NO₂ column
94 densities (refer to section 4 for details) into a neural Network model (GeoNet), to forecast full-
95 coverage surface NO₂ concentration over the next day from the current time t (i.e., $t+24h$).
96 Compared with previous air quality forecasting based on the simulation of atmospheric physics
97 and chemistry possibly combined with data assimilation approaches, GeoNet relies solely on
98 geostationary satellite measurements and ancillary meteorology data. GeoNet effectively
99 addresses the complex nonlinear relationships between future short-term air quality and current
100 satellite observations, as well as temporally adjacent meteorological variables (C. Zhang et al.,
101 2022). The method employs satellite and meteorological variables within the spatial vicinity of
102 individual air quality monitoring sites as input features, with site observations serving as labels
103 for model training. The resulting model achieves accurate and comprehensive air quality
104 predictions across the entire domain over East China, which is a significant achievement given
105 that past machine learning technologies have relied on only a few stations or polar-orbiting
106 satellite observations.

107 **2 Materials and Methods**

108 **2.1 Geostationary satellite observations of atmospheric NO₂**

109 GEMS is the first UV-Vis spectrometer at a geostationary satellite orbit, measuring
110 atmospheric pollutants such as NO₂, SO₂, O₃, and HCHO over East Asia, at a spatial resolution
111 of 3.5 km × 7.5 km at nadir and a temporal resolution of 1 hour during the daytime (J. Kim et
112 al., 2020). Based on the unique spectral absorption of trace gases, the atmospheric NO₂ column
113 can be retrieved in visible wavelengths from the spectra of back-scattered sunlight. The details
114 of the GEMS NO₂ retrieval can be found in the Algorithm Theoretical Basis Document
115 (available at <https://nesc.nier.go.kr/ko/html/satellite/doc/doc.do>, last access: June 1, 2023). In
116 this study, we used the tropospheric NO₂ column from the GEMS NO₂ version 2.0 product, as



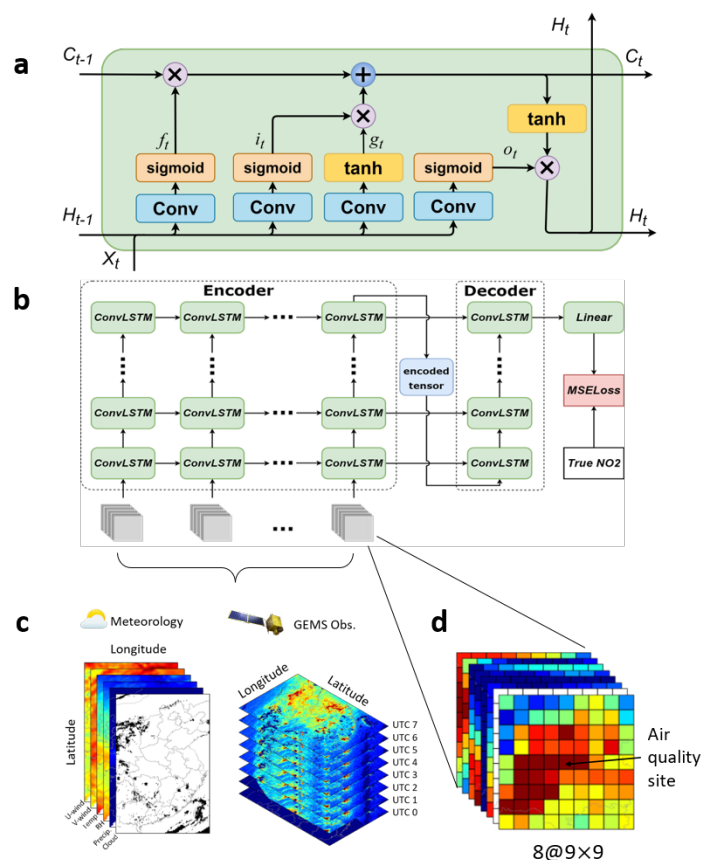
117 well as the cloud fraction for each satellite ground pixel. Overall, GEMS NO₂ measurements
118 have a good correlation with ground-based remote sensing instruments, with correlation
119 coefficients (R) between 0.69-0.81, and root mean square of errors (RMSE) between 3.2-
120 4.9×10^{15} molecules/cm² (S. Kim et al., 2023).

121 **2.2 Ancillary datasets**

122 Other input information including meteorological datasets is necessary to better constrain
123 the prediction of future NO₂ pollution. Here, both the ERA5 meteorology reanalysis (Hersbach
124 et al., 2020) and the CAMS forecast (Peuch et al., 2022) were used to provide meteorological
125 parameters such as zonal and meridional wind (U-wind and V-wind), temperature (Temp),
126 relative humidity (RH), and precipitation (Precip). In addition, the fraction of cloud cover
127 available from the satellite NO₂ datasets was also considered. To fill the missing gaps in the
128 satellite NO₂ measurements, we use both the NO₂ concentrations from the WRF-Chem model
129 (C. Zhang et al., 2022) and the CAMS forecast of atmospheric composition. Note that the
130 reanalysis datasets were typically updated with a week delay from real-time, while the forecast
131 datasets can provide future 7-day meteorology from the current time. Therefore, the latency of
132 input datasets would affect the operational prediction of the GeoNet model. Surface NO₂
133 measurements were used as the ground-truth label in the model training phase, available from
134 over 1000 national air quality sites by the China National Environmental Monitoring Centre
135 (CNEMC) (Kong et al., 2021).

136 The preprocessing steps of model input datasets, including outlier detection, missing value
137 handling, resampling, and normalization, are described in Supplementary Text S1.

138 **2.3 The GeoNet model**



139

140 **Figure 1.** The framework of predicting surface NO₂ map based on Geostationary satellite measurements and
 141 a ConvLSTM neural network model (GeoNet). (a) the structure of the ConvLSTM block; (b) a diagram of
 142 GeoNet model structure with inputs and output; (c) an illustration of the model input parameters including
 143 meteorological variables and hourly NO₂ measurements by the Geostationary satellite; (d) the input data
 144 cube of different features for single training batch, which is centered at an air quality site.

145 Fig. 1 illustrates the structure and methodology of the artificial intelligence air quality
 146 forecasting model established in this study. Given the distinctive nature of spatiotemporal
 147 sequence data for air quality, predictions must consider not only temporal relationships but also
 148 spatial correlations. The deep learning model employed in this research utilizes convolutional
 149 long short-term memory (ConvLSTM) as its kernel, a variant of the LSTM model designed for
 150 the time series forecasting (Lin et al., 2020). It incorporates a convolutional network structure
 151 to capture spatial features of three-dimensional inputs. Both input-to-state and state-to-state



152 transitions involve convolutional structures. ConvLSTM determines the future state of a unit
153 within a grid based on inputs from its local neighbors and past states, allowing it to effectively
154 model the spatiotemporal dynamics of air quality. The ConvLSTM kernel structure employed
155 in training is illustrated in Fig. 5a. Here, X_t represents the input at time t , H_t and H_{t-1} denote
156 the outputs at times t and $t-1$, and C_t and C_{t-1} represent the states at times t and $t-1$. The
157 computational process is as follows:

$$158 \quad i_t = \sigma(X_t * w_{xi} + H_{t-1} * w_{hi} + b_i) \quad (1)$$

$$159 \quad f_t = \sigma(X_t * w_{xf} + H_{t-1} * w_{hf} + b_f) \quad (2)$$

$$160 \quad o_t = \sigma(X_t * w_{xo} + H_{t-1} * w_{ho} + b_o) \quad (3)$$

$$161 \quad g_t = \tanh(X_t * w_{xg} + H_{t-1} * w_{hg} + b_g) \quad (4)$$

$$162 \quad C_t = f_t \times C_{t-1} + i_t \times g_t \quad (5)$$

$$163 \quad H_t = o_t \times \tanh(C_t) \quad (6)$$

164 Where the asterisk (*) represents the convolution operator, w is the convolution kernel, b is the
165 offset, \tanh is the hyperbolic tangent function, and σ is the activation function of Sigmoid.

166 The model primarily consists of three components: an encoder, a decoder, and fully
167 connected layers. Tropospheric NO_2 observations from the GEMS satellite for different
168 consecutive hours within a day, along with corresponding meteorological forecast field data,
169 serve as input features for model training. The encoder processes the spatiotemporal sequences
170 of input features for the preceding 8 hours ($t-7\text{h}$, $t-6\text{h}$, ..., t), which are then decoded by the
171 decoder. The final output, representing NO_2 concentrations at 4-hour intervals for the next 24
172 hours ($t+4\text{h}$, $t+8\text{h}$, $t+12\text{h}$, ..., $t+24\text{h}$), is produced through fully connected layers. The loss
173 function of mean squared error (MSE) is calculated by comparing the model output with the
174 actual values from station observations, and the model undergoes iterative training. In the
175 training task for a single station sample, the model utilizes continuous and distinct hourly
176 dynamic images of all variables within the spatiotemporal vicinity of the station as input (see



177 Fig. 1c-d). This effectively considers the intricate correlations in time and space between air
178 quality, satellite observations, and meteorological input features. The performance metrics
179 such as the coefficient of determination (R^2), root mean square of error (RMSE), mean absolute
180 error (MAE), and mean absolute percentage error (MAPE), were used to diagnose the model
181 (see definition in Supplementary Text S2). The model configuration and optimization are also
182 described in detail in Supplementary Text S2.

183 **2.4 The importance of the model input feature**

184 Permutation feature importance is a technique used to assess the significance of each input
185 feature in a machine-learning model (Altmann et al., 2010). The core idea is to evaluate the
186 impact of each feature on model performance by randomly shuffling its values and observing
187 the resulting change in the model's accuracy. In this study, for each input feature of the GeoNet,
188 we iteratively shuffle its value independently while keeping other features unchanged, and then
189 observe the model prediction on the modified input. The difference in the model prediction
190 performance between using the original and shuffling input quantifies the feature's importance.
191 Here, we measure the relative importance of each input feature using the metric of $1-R^2$, due
192 to its good standardized and indicative ability (C. Zhang et al., 2022). Generally, a larger
193 performance drop indicates greater importance, as the model heavily relies on that feature for
194 predictions. Conversely, smaller drops or increases suggest the feature may be less crucial or
195 redundant. By permuting the input feature array based on the different spatial and temporal
196 domains, we can gain a deeper understanding of how feature importance varies spatially and
197 temporally. For example, the relative importance of one meteorology variable may vary with
198 different diurnal, weekly, and monthly cycles, revealing the variability of its impact on the
199 predicted NO_2 levels.

200 **3 Results and Discussion**

201 **3.1 Model performance**

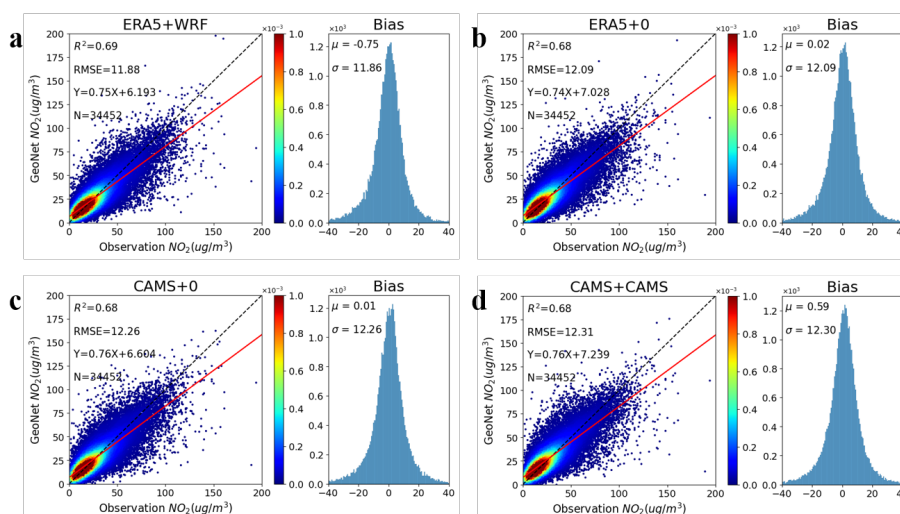


202 Based on the GeoNet model and necessary input data (refer to section 2), we have
203 achieved preliminary predictions of near-surface NO₂ concentration with full spatial coverage
204 and a spatial resolution of 0.01 degrees over eastern China, at four-hour intervals over the next
205 24 hours. In this study, we first tested the impact of using reanalysis and forecast meteorology
206 datasets and filling in missing values in satellite observation data on the model predictions.
207 Meteorological data sources included ERA5 reanalysis meteorology datasets with a latency of
208 one week, and CAMS forecast meteorology data for the upcoming 7 days. The reanalysis
209 datasets usually have higher precision than the forecast. Previous studies revealed that the
210 accuracy of the information on meteorology and chemical composition significantly affects the
211 performance of machine learning models in estimating air pollutant concentrations (Wang et
212 al., 2024; Zuo et al., 2023). Due to the shielding effect of clouds, a considerable proportion of
213 missing values may even exist in satellite NO₂ observations. Recent air quality big-data
214 research usually requires the gap-filling of missing satellite data before inputting it into the
215 machine learning model, either by spatial interpolation or regression techniques (M. Kim et al.,
216 2021). We tested three methods for handling missing data, such as setting them to a fill value
217 of zero, or replacing them by real-time CAMS simulated NO₂, or WRF-Chem simulated NO₂
218 results (not real-time, but with higher precision).

219 The comparison results to the validation datasets (10% of whole datasets, randomly
220 sampled) indicate that the scenario with the “weakest” input, i.e., using CAMS meteorology
221 datasets and replacing missing satellite NO₂ data with fill-values (Fig. 2c), corresponds to the
222 NO₂ prediction metrics of R²=0.68 and RMSE=12.26 µg/m³. In contrast, the strongest
223 configuration, using ERA-5 reanalysis meteorology and imputing with WRF-Chem
224 simulations (Fig. 2a), corresponds to the prediction performance of R²=0.69 and RMSE=11.88
225 µg/m³. To compromise between the performance of real-time and accuracy, we selected the
226 configuration scenario of using CAMS meteorology and imputing with CAMS NO₂ (Fig. 2d)



227 for subsequent discussion and operational forecasting, with an $R^2=0.68$ and $RMSE=12.31$
 228 $\mu\text{g}/\text{m}^3$. In summary, the use of higher-precision meteorology and filling missing NO_2 data
 229 enhances the model's prediction accuracy on the validation dataset, but to a rather limited
 230 extent. This suggests that, unlike previous machine learning techniques, GeoNet can effectively
 231 adapt to three-dimensional inputs of varying accuracy and type, fully explore the
 232 spatiotemporal correlation of data features, and demonstrate strong model generalization
 233 capabilities.



234

235 **Figure 2.** The GeoNet prediction performance of the surface NO_2 concentration compared to the validation
 236 samples, based on different input datasets of meteorology and atmospheric composition: (a) use ERA5
 237 meteorology and fill satellite measurement gaps with WRF-Chem simulated NO_2 ; (b) use ERA5
 238 meteorology and NO_2 fill-value of zero for over gaps; (c) use CAMS meteorology and NO_2 fill-value of zero
 239 for gaps; (d) use CAMS meteorology and CAMS NO_2 . The left plot shows the scatter comparisons between
 240 GeoNet predictions and site observations, while the right plot shows the bias distribution between the two.

241 Figs. S5-S8 provide an overview of the major metrics (e.g., R^2 , RMSE, MAE, and MPE)
 242 of GeoNet prediction performance varying with prediction hours from t+4h to t+24h in
 243 different months. The results indicate that the model exhibits a higher correlation in NO_2
 244 forecast during the spring and winter seasons compared to the summer, while the RMSE errors
 245 show the opposite trend. This could be attributed to much higher NO_2 pollution levels in winter



246 months. Additionally, GeoNet's NO₂ prediction errors gradually increase during the next 24
247 hours, particularly after t+20h. This is primarily due to the short lifetime of atmospheric NO₂,
248 leading to a diminishing constraint from historical observational data on future NO₂ predictions.
249 Similar phenomena are also observed in machine learning or model-assisted weather forecasts
250 (Andersson et al., 2021).

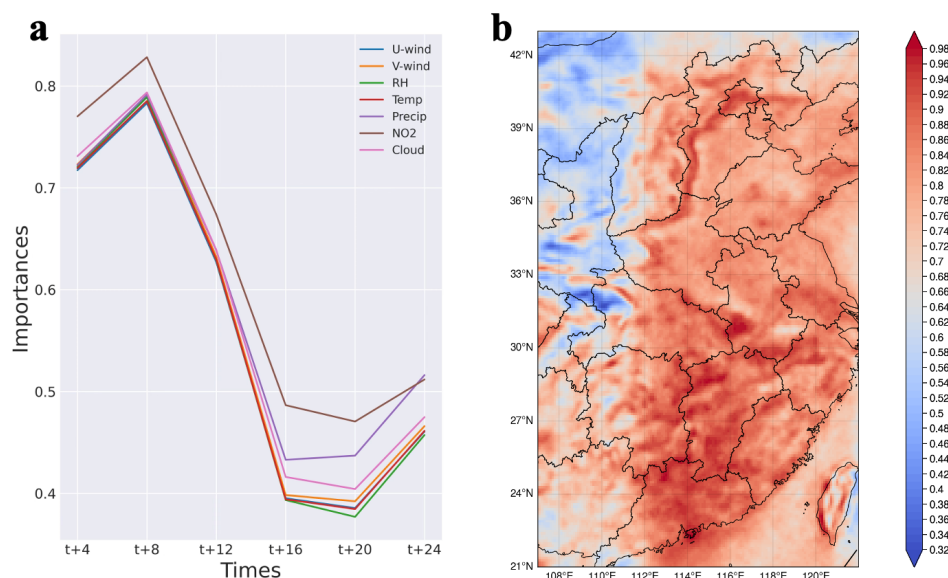
251 To assess the GeoNet model's performance for short-term pollution events, we compared
252 it with near-surface NO₂ from CAMS forecasts, and in situ observations from CNEMC ground
253 stations. Fig. S9 illustrates the daily time series of t+4h NO₂ from GeoNet, CAMS, and
254 CNEMC for three typical sites in Beijing, Shanghai, and Guangzhou in 2021. As shown from
255 the plot, NO₂ predictions by both GeoNet and CAMS generally agreed with the variation trends
256 of CNEMC measurement. However, CAMS forecasts systematically overestimate the surface
257 NO₂ concentration by 100%, possibly resulting from the biases in the NO_x emission inventory
258 (Douros et al., 2023). Compared to CAMS, the GeoNet prediction closely aligns with the
259 ground-truth observations at CNEMC sites over eastern China, with an overall R² > 0.5 and
260 mean bias < 5 µg/m³ for polluted regions (see Fig. S10 and S11, respectively).

261 **3.2 Main factors in NO₂ forecast and their implications**

262 Previous physics-based numeric models of air quality prediction, e.g., the CAMS global
263 forecast model and the regional WRF-CMAQ model (Kuhn et al., 2024; Kumar et al., 2021;
264 Liu et al., 2023), can simulate the atmospheric physical and chemical processes (such as
265 advection, diffusion, deposition, and chemical reactions) by solving the atmospheric equations.
266 Recent data assimilation techniques further take real-time monitoring data from satellite and
267 ground-based platforms as model constraints to better predict air quality variables (Antje Inness
268 et al., 2022). Compared with physics-based models, "black-box" models such as the deep
269 learning technique usually lack interpretability and explainability (Q.-s. Zhang & Zhu, 2018).
270 This hinders the understanding and implications for predicting air quality variables such as



271 NO₂. Here, we measure the relative importance of each input feature on the NO₂ forecast
 272 accuracy, by iteratively permuting the input array and observing its influences on the model
 273 prediction.



274
 275 **Figure 3.** (a) The overall relative importance of different input features such as wind, surface pressure,
 276 satellite NO₂, and cloud mask, in GeoNet NO₂ forecast, varying with different hour steps from t+4h to t+24h.
 277 (b) The spatial distribution of the relative importance of satellite NO₂ measurements in the GeoNet NO₂
 278 forecast in 2021.

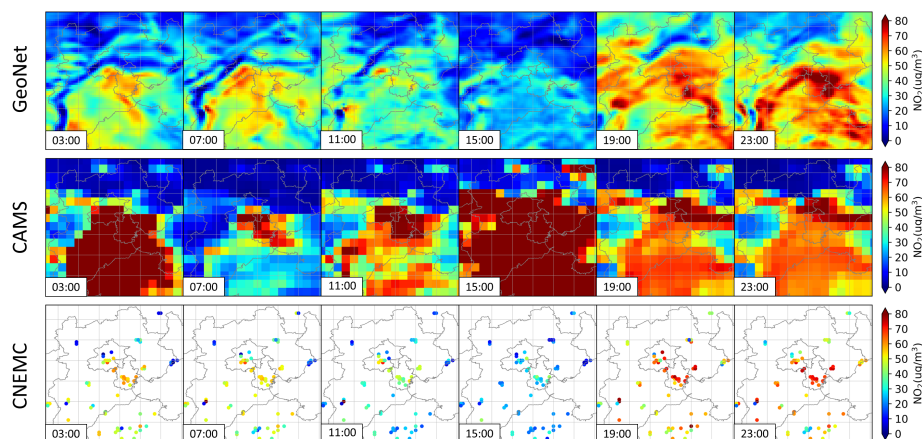
279 Fig. 3a presents the relative importance ($1-R^2$) of different input features varying with
 280 prediction hour steps from t+4h to t+24h. The geostationary satellite NO₂ measurements play
 281 the highest role in predicting surface NO₂ levels of the next day, although it degrades after t+8h.
 282 Other meteorological input features also show a major impact on NO₂ prediction performance.
 283 By permutating the input array for each ground pixel, Fig. 3b derived the spatial distribution
 284 of the relative importance of geostationary satellite NO₂ in the predicting performance. Overall,
 285 satellite NO₂ has a higher impact in densely populated areas experiencing severe air pollution,
 286 such as the Pearl River Delta, Yangtze River Delta, and Jianghuai Plain, than in western China.



287 Such results highlight the underappreciated role of satellite NO₂ measurements with high
288 spatial and temporal coverage in air pollution forecasts.

289 **3.3 NO₂ pollution episodes and health exposure forecast**

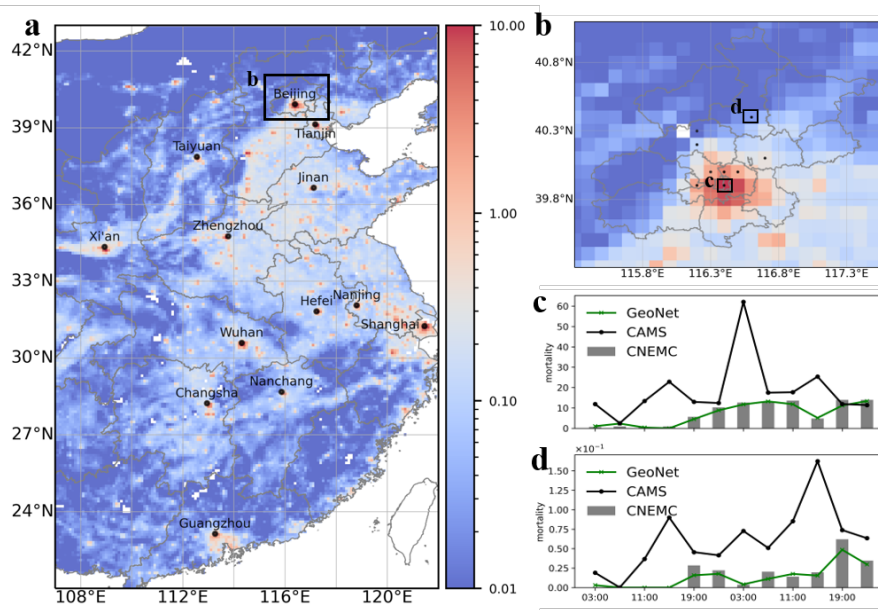
290 Beyond its prediction accuracy, GeoNet exhibits a pronounced advantage in spatial
291 coverage and resolution, allowing for capturing finer-scale details in the pollutant distribution.
292 Illustrated in Fig. S12, GeoNet demonstrates remarkable performance in predicting spatial
293 nuances of NO₂ pollution, particularly when contrasted with ground-based and satellite
294 observations. During a typical winter NO₂ pollution event (as shown in Fig. 4), GeoNet
295 accurately simulates a significant decrease in concentrations at 11:00 and 15:00, probably led
296 by intense photochemical activity in the daytime, coincident with ground-based observations.
297 It also outperforms CAMS in predicting NO₂ variations throughout the day. The GeoNet model
298 also retains the distributional differences in NO₂ concentrations between urban and rural areas,
299 consistent with emission source characteristics and satellite observations. The suboptimal
300 performance of CAMS predictions can be attributed to insufficient observational constraints
301 and the use of outdated emission inventories (Douros et al., 2023). In the European region, the
302 assimilation of TROPOMI observations into CAMS forecasts significantly improves the
303 simulation accuracy of near-surface NO₂ concentrations and tropospheric column densities (A.
304 Inness et al., 2019). Neural network methods, similar to GeoNet, could be used to correct and
305 downscale forecast results by existing models (Baghanam et al., 2024). This approach holds
306 promise for achieving operational air quality forecasts that balance efficiency and accuracy.



307

308 **Figure 4.** The spatial distribution comparisons of surface NO₂ concentration between (a) GeoNet prediction,
309 (b) CAMS prediction, and (c) ground-based CNEMC site measurements. Note that the results are presented
310 for different continuing local hours (labeled text in the subplot) on 23 November 2021.

311 In this study, we used a simplified linearized risk model for the short-term NO₂ exposure
312 (Meng et al., 2021; C. Zhang et al., 2022) to calculate the distribution of all-cause mortality
313 risks based on GeoNet NO₂ predictions (see Fig. 5). Short-term NO₂ exposure leads to
314 remarkable regional differences in all-cause mortality, which are mainly concentrated in highly
315 polluted and densely populated urban areas. For both urban and suburban locations in Beijing
316 (see Fig. 5c-d), GeoNet-based NO₂ pollution exposure predictions are more consistent with
317 actual in situ observations than the CAMS forecasts. Current air quality health indices
318 forecasting based on limited station data has significant gaps, making it difficult to meet the
319 refined needs for different populations in urban, suburban, and rural areas. Integrating GeoNet
320 forecasts based on hourly geostationary satellite observations can support spatially
321 comprehensive and fine-scale air quality health risk prediction. This, in turn, guides managing
322 the risks of air pollution exposure-related diseases in sensitive populations and communities.



323

324 **Figure 5.** Mortality risk of short-term NO₂ exposure based on the GeoNet prediction on November 23, 2021.
 325 (a) mean mortality due to the predicted NO₂ exposure in East China; (b) a zoom-in map over Beijing and its
 326 neighboring area; (c) and (d) are comparisons of mortality estimation over the Beijing urban and rural
 327 regions (the rectangle areas presented in b), respectively, based on different NO₂ exposure prediction among
 328 GeoNet, CAMS, and CNEMC.

329 4 Conclusion

330 The GeoNet model utilizes the unprecedented hourly air quality observations from
 331 geostationary satellites and resolves nonlinear associations in spatiotemporal proximity across
 332 multiple data sources. It achieves seamless short-term regional air quality predictions,
 333 exhibiting significant performance advantages over existing machine-learning air quality
 334 prediction models. To strike a balance between real-time and accuracy requirements, we
 335 evaluated the impact of using reanalysis- and forecast-based meteorology datasets, as well as
 336 imputing the missing values of satellite NO₂. The findings reveal that the GeoNet model
 337 demonstrates robust generalization across diverse datasets, with minimal fluctuations in
 338 prediction performance. Overall, the model achieves an RMSE of 12.31 μg/m³ and an R² of
 339 0.68 in predicting NO₂ concentrations every 4 hours for the next 24 hours. However, validation



340 accuracy notably diminishes after t+16h within the next 24 hours, with stronger predictive
341 correlations observed in seasons characterized by severe pollution, such as spring and winter,
342 compared to summer.

343 Compared to traditional chemical model forecasts and data assimilation predictions, the
344 GeoNet model handles various data sources, including meteorological simulations and air
345 quality observations, and more accurately captures spatial intricacies of air pollution evolution.
346 The GeoNet framework elucidated in this study forecasts short-term near-surface NO₂
347 concentrations and demonstrates transferable learning potentials for predicting other pollutants.
348 In our forthcoming endeavors, we aim to enhance the predictability of near-surface ozone and
349 particulate matter pollution by integrating GEMS observations of tropospheric ozone and its
350 precursors like NO₂ and HCHO. This study underscores the pivotal role of next-generation
351 stationary satellite observations of air pollution constituents in air quality forecasting, with the
352 potential to advance operational air quality forecasting and mitigate associated health risks by
353 integrating machine learning technologies.

354



355 **Data and code availability.** The GEMS NO₂ v2.0 data is available from the National Institute
356 of Environmental Research (NIER) of South Korea (<https://nesc.nier.go.kr/en/html/index.do>,
357 last access: December 10, 2023). We downloaded the NO₂ measurements from the CNEMC
358 real-time air quality platform (<https://air.cnemc.cn:18007/>, last access: Jun 8, 2023). ERA-5
359 reanalysis meteorological data is obtained from the European Center for Medium-Range
360 Weather Forecasts (<https://climate.copernicus.eu/climate-reanalysis>, last access: December 8,
361 2023). CAMS forecast of meteorological and atmospheric NO₂ datasets are retrieved from the
362 CAMS Atmosphere Data Store (<https://ads.atmosphere.copernicus.eu/>, last access: December
363 8, 2023). The source codes of the GeoNet model, surface NO₂ prediction, and necessary input
364 data can be obtained from Chengxin Zhang (zcx2011@ustc.edu.cn) upon reasonable request.

365

366 **Contributions:** C.Z. implemented the GeoNet model and analyzed the data. C.L. supervised
367 the study. C.Z. wrote the manuscript with input from all co-authors.

368

369 **Competing interests:** The contact author has declared that none of the authors has any
370 competing interests.

371

372 **Acknowledgments.** This study was supported by the National Natural Science Foundation of
373 China (Nos. 42225504, 62305322, and 42375120), the National Key Research and
374 Development Program of China (Nos. 2022YFC3700100 and 2023YFC3706104) and the New
375 Cornerstone Science Foundation through the XPLORER PRIZE (2023-1033).

376

377 **References**

- 378 Altmann, A., Tolosi, L., Sander, O., & Lengauer, T. (2010). Permutation importance: a
379 corrected feature importance measure. *Bioinformatics*, 26(10), 1340-1347.
380 <https://www.ncbi.nlm.nih.gov/pubmed/20385727>
- 381 Andersson, T. R., Hosking, J. S., Pérez-Ortiz, M., Paige, B., Elliott, A., Russell, C., et al.
382 (2021). Seasonal Arctic sea ice forecasting with probabilistic deep learning. *Nature*
383 *Communications*, 12(1), 5124.
- 384 Baghanam, A. H., Nourani, V., Bejani, M., Pourali, H., Kantoush, S. A., & Zhang, Y. (2024).
385 A systematic review of predictor screening methods for downscaling of numerical
386 climate models. *Earth-Science Reviews*, 104773.
- 387 Bi, K., Xie, L., Zhang, H., Chen, X., Gu, X., & Tian, Q. (2023). Accurate medium-range
388 global weather forecasting with 3D neural networks. *Nature*, 1-6.
- 389 Boukabara, S.-A., Krasnopolsky, V., Penny, S. G., Stewart, J. Q., McGovern, A., Hall, D., et
390 al. (2020). Outlook for exploiting artificial intelligence in the earth and environmental
391 sciences. *Bulletin of the American Meteorological Society*, 1-53.
- 392 Campbell, P. C., Tang, Y., Lee, P., Baker, B., Tong, D., Saylor, R., et al. (2022).
393 Development and evaluation of an advanced National Air Quality Forecasting
394 Capability using the NOAA Global Forecast System version 16. *Geoscientific Model*
395 *Development*, 15(8), 3281-3313.
- 396 Chan, K. L., Valks, P., Heue, K.-P., Lutz, R., Hedelt, P., Loyola, D., et al. (2023). Global
397 Ozone Monitoring Experiment-2 (GOME-2) daily and monthly level-3 products of
398 atmospheric trace gas columns. *Earth System Science Data*, 15(4), 1831-1870.
- 399 Douros, J., Eskes, H., van Geffen, J., Boersma, K. F., Compernelle, S., Pinardi, G., et al.
400 (2023). Comparing Sentinel-5P TROPOMI NO₂ column observations with the
401 CAMS regional air quality ensemble. *Geoscientific Model Development*, 16(2), 509-
402 534.



- 403 Du, S., Li, T., Yang, Y., & Horng, S. J. (2021). Deep Air Quality Forecasting Using Hybrid
404 Deep Learning Framework. *IEEE Transactions on Knowledge and Data Engineering*,
405 33(6), 2412-2424.
- 406 Guarin, J. R., Jägermeyr, J., Ainsworth, E. A., Oliveira, F. A., Asseng, S., Boote, K., et al.
407 (2024). Modeling the effects of tropospheric ozone on the growth and yield of global
408 staple crops with DSSAT v4. 8.0. *Geoscientific Model Development*, 17(7), 2547-
409 2567.
- 410 Hersbach, H., Bell, B., Berrisford, P., Hirahara, S., Horányi, A., Muñoz-Sabater, J., et al.
411 (2020). The ERA5 global reanalysis. *Quarterly Journal of the Royal Meteorological
412 Society*, 146(730), 1999-2049.
413 <https://rmets.onlinelibrary.wiley.com/doi/abs/10.1002/qj.3803>
- 414 Hong, C., Zhang, Q., Zhang, Y., Davis, S. J., Tong, D., Zheng, Y., et al. (2019). Impacts of
415 climate change on future air quality and human health in China. *Proceedings of the
416 National Academy of Sciences*, 116(35), 17193-17200.
- 417 Hsu, C. H., Henze, D. K., Mizzi, A. P., González Abad, G., He, J., Harkins, C., et al. (2024).
418 An Observing System Simulation Experiment Analysis of How Well Geostationary
419 Satellite Trace-Gas Observations Constrain NO_x Emissions in the US. *Journal of
420 Geophysical Research: Atmospheres*, 129(2), e2023JD039323.
- 421 Inness, A., Aben, I., Ades, M., Borsdorff, T., Flemming, J., Jones, L., et al. (2022).
422 Assimilation of S5P/TROPOMI carbon monoxide data with the global CAMS near-
423 real-time system. *Atmospheric Chemistry and Physics*, 22(21), 14355-14376.
- 424 Inness, A., Flemming, J., Heue, K. P., Lerot, C., Loyola, D., Ribas, R., et al. (2019).
425 Monitoring and assimilation tests with TROPOMI data in the CAMS system: near-
426 real-time total column ozone. *Atmospheric Chemistry and Physics*, 19(6), 3939-3962.
427 <Go to ISI>://WOS:000462793200001
- 428 Irrgang, C., Boers, N., Sonnewald, M., Barnes, E. A., Kadow, C., Staneva, J., & Saynisch-
429 Wagner, J. (2021). Towards neural Earth system modelling by integrating artificial
430 intelligence in Earth system science. *Nature Machine Intelligence*, 3(8), 667-674.
- 431 Kim, J., Jeong, U., Ahn, M.-H., Kim, J. H., Park, R. J., Lee, H., et al. (2020). New era of air
432 quality monitoring from space: Geostationary Environment Monitoring Spectrometer
433 (GEMS). *Bulletin of the American Meteorological Society*, 101(1), E1-E22.
- 434 Kim, M., Brunner, D., & Kuhlmann, G. (2021). Importance of satellite observations for high-
435 resolution mapping of near-surface NO₂ by machine learning. *Remote Sensing of
436 Environment*, 264, 112573. <Go to ISI>://WOS:000688451300002
- 437 Kim, S., Kim, D., Hong, H., Chang, L.-S., Lee, H., Kim, D.-R., et al. (2023). First-time
438 comparison between NO₂ vertical columns from Geostationary Environmental
439 Monitoring Spectrometer (GEMS) and Pandora measurements. *Atmospheric
440 Measurement Techniques*, 16(16), 3959-3972.
- 441 Kong, L., Tang, X., Zhu, J., Wang, Z. F., Li, J. J., Wu, H. J., et al. (2021). A 6-year-long
442 (2013-2018) high-resolution air quality reanalysis dataset in China based on the
443 assimilation of surface observations from CNEMC. *Earth System Science Data*,
444 13(2), 529-570. <Go to ISI>://WOS:000622997600001
- 445 Kuhn, L., Beirle, S., Kumar, V., Osipov, S., Pozzer, A., Bösch, T., et al. (2024). On the
446 influence of vertical mixing, boundary layer schemes, and temporal emission profiles
447 on tropospheric NO₂ in WRF-Chem—comparisons to in situ, satellite, and MAX-
448 DOAS observations. *Atmospheric Chemistry and Physics*, 24(1), 185-217.
- 449 Kumar, V., Remmers, J., Beirle, S., Fallmann, J., Kerkweg, A., Lelieveld, J., et al. (2021).
450 Evaluation of the coupled high-resolution atmospheric chemistry model system
451 MECO (n) using in situ and MAX-DOAS NO₂ measurements. *Atmospheric
452 Measurement Techniques*, 14(7), 5241-5269.



- 453 Lam, R., Sanchez-Gonzalez, A., Willson, M., Wirnsberger, P., Fortunato, M., Alet, F., et al.
454 (2023). Learning skillful medium-range global weather forecasting. *Science*,
455 382(6677), 1416-1421.
- 456 Lin, Z., Li, M., Zheng, Z., Cheng, Y., & Yuan, C. (2020). *Self-attention convlstm for*
457 *spatiotemporal prediction*. Paper presented at the Proceedings of the AAAI
458 conference on artificial intelligence.
- 459 Liu, C., Wu, C., Kang, X., Zhang, H., Fang, Q., Su, Y., et al. (2023). Evaluation of the
460 prediction performance of air quality numerical forecast models in Shenzhen.
461 *Atmospheric Environment*, 314, 120058.
462 <https://www.sciencedirect.com/science/article/pii/S1352231023004843>
- 463 Makar, P., Gong, W., Milbrandt, J., Hogrefe, C., Zhang, Y., Curci, G., et al. (2015).
464 Feedbacks between air pollution and weather, Part 1: Effects on weather. *Atmospheric*
465 *Environment*, 115, 442-469.
- 466 Manisalidis, I., Stavropoulou, E., Stavropoulos, A., & Bezirtzoglou, E. (2020).
467 Environmental and health impacts of air pollution: a review. *Frontiers in public*
468 *health*, 14.
- 469 Meng, X., Liu, C., Chen, R., Sera, F., Vicedo-Cabrera, A. M., Milojevic, A., et al. (2021).
470 Short term associations of ambient nitrogen dioxide with daily total, cardiovascular,
471 and respiratory mortality: multilocation analysis in 398 cities. *bmj*, 372.
- 472 Nguyen, T., Brandstetter, J., Kapoor, A., Gupta, J. K., & Grover, A. (2023). ClimaX: A
473 foundation model for weather and climate. *arXiv preprint arXiv:2301.10343*.
- 474 Peuch, V.-H., Engelen, R., Rixen, M., Dee, D., Flemming, J., Suttie, M., et al. (2022). The
475 Copernicus Atmosphere Monitoring Service: From Research to Operations. *Bulletin*
476 *of the American Meteorological Society*, 103(12), E2650-E2668.
- 477 Sathe, Y., Gupta, P., Bawase, M., Lamsal, L., Patadia, F., & Thipse, S. (2021). Surface and
478 satellite observations of air pollution in India during COVID-19 lockdown:
479 Implication to air quality. *Sustainable cities and society*, 66, 102688.
- 480 Shah, V., Jacob, D. J., Li, K., Silvern, R. F., Zhai, S., Liu, M., et al. (2020). Effect of
481 changing NO_x lifetime on the seasonality and long-term trends of satellite-observed
482 tropospheric NO₂ columns over China. *Atmospheric Chemistry and Physics*, 20(3),
483 1483-1495.
- 484 Shu, L., Zhu, L., Bak, J., Zoogman, P., Han, H., Liu, S., et al. (2023). Improving ozone
485 simulations in Asia via multisource data assimilation: results from an observing
486 system simulation experiment with GEMS geostationary satellite observations.
487 *Atmospheric Chemistry and Physics*, 23(6), 3731-3748.
- 488 Van Geffen, J., Eskes, H., Compernelle, S., Pinardi, G., Verhoelst, T., Lambert, J.-C., et al.
489 (2022). Sentinel-5P TROPOMI NO₂ retrieval: impact of version v2. 2 improvements
490 and comparisons with OMI and ground-based data. *Atmospheric Measurement*
491 *Techniques*, 15(7), 2037-2060.
- 492 Wang, S., Zhang, M., Gao, Y., Wang, P., Fu, Q., & Zhang, H. (2024). Diagnosing drivers of
493 PM_{2.5} simulation biases in China from meteorology, chemical composition, and
494 emission sources using an efficient machine learning method. *Geoscientific Model*
495 *Development*, 17(9), 3617-3629.
- 496 Zhang, C., Liu, C., Li, B., Zhao, F., & Zhao, C. (2022). Spatiotemporal neural network for
497 estimating surface NO₂ concentrations over north China and their human health
498 impact. *Environmental Pollution*, 119510.
- 499 Zhang, Q.-s., & Zhu, S.-C. (2018). Visual interpretability for deep learning: a survey.
500 *Frontiers of Information Technology & Electronic Engineering*, 19(1), 27-39.



- 501 Zhong, S., Zhang, K., Bagheri, M., Burken, J. G., Gu, A., Li, B., et al. (2021). Machine
502 learning: new ideas and tools in environmental science and engineering.
503 *Environmental Science & Technology*, 55(19), 12741-12754.
504 Zuo, C., Chen, J., Zhang, Y., Jiang, Y., Liu, M., Liu, H., et al. (2023). Evaluation of four
505 meteorological reanalysis datasets for satellite-based PM_{2.5} retrieval over China.
506 *Atmospheric Environment*, 305, 119795.
507
508